Two-photon photodissociation dynamics study of CS₂: The S(¹S) atom channel ⊘

Shuaikang Yang ^⑤; Zhiguo Zhang [☑] ^⑤; Yongxin Dong; Zijie Luo; Wei Hua; Zhenxing Li [☑]; Quan Shuai ^⑤; Xingan Wang ^⑥; Kaijun Yuan [☑] ^⑥; Xueming Yang



J. Chem. Phys. 163, 044307 (2025) https://doi.org/10.1063/5.0283135





Articles You May Be Interested In

Photodissociation dynamics of nitrous oxide: The O (1 D) + N 2 (X 1 Σ g +) product channel

Chin. J. Chem. Phys. (April 2024)

Ion velocity map imaging study of the charge transfers from ${\rm N_2}^+\!/{\rm N}^+$ to ${\rm H_2O}$

J. Chem. Phys. (April 2025)

Polarization diagnosis and transmission distortion calibration of the Dalian coherent light source

Rev. Sci. Instrum. (July 2025)





Two-photon photodissociation dynamics study of CS₂: The S(¹S) atom channel

Cite as: J. Chem. Phys. 163, 044307 (2025); doi: 10.1063/5.0283135

Submitted: 29 May 2025 • Accepted: 7 July 2025 •

Published Online: 24 July 2025







Shuaikang Yang,^{1,2} D Zhiguo Zhang,^{2,3,a)} D Yongxin Dong,² Zijie Luo,² Wei Hua,² Zhenxing Li,^{2,4,a)} Quan Shuai,² D Xingan Wang,¹ Kaijun Yuan,^{2,5,a)} and Xueming Yang^{2,5,6}

AFFILIATIONS

- Department of Chemical Physics, School of Chemistry and Materials Science, University of Science and Technology of China, Hefei, Anhui 230026, China
- 2 State Key Laboratory of Chemical Reaction Dynamics and Dalian Coherent Light Source, Dalian Institute of Chemical Physics, Chinese Academy of Sciences, Dalian, Liaoning 116023, China
- ³ Key Laboratory of Functional Materials and Devices for Informatics of Anhui Higher Education Institutions and School of Physics and Electronic Engineering, Fuyang Normal University, Fuyang, Anhui 236041, China
- Institute of Advanced Light Source Facilities, Shenzhen 518107, China
- ⁵Hefei National Laboratory, Hefei 230088, China
- Department of Chemistry and Center for Advanced Light Source Research, College of Science, Southern University of Science and Technology, Shenzhen 518055, China
- ^{a)}Authors to whom correspondence should be addressed: zhgzhang@mail.ustc.edu.cn; lizhenxing@mail.iasf.ac.cn; and kjyuan@dicp.ac.cn

ABSTRACT

Two-photon photodissociation dynamics of carbon disulfide (CS₂) were studied by means of the sliced velocity map ion imaging technique. The $S(^1S) + CS(X^1\Sigma^+)$ channel was directly observed from the measured images of $S(^1S)$ products in the wavelength range of 290.10-336.88 nm. The translational energy distributions and angular distributions of fragments have been derived. Rovibrational states of the $CS(X^1\Sigma^+)$ co-products were partially resolved in the translational energy spectra and can be populated up to the energy limit of the available energy. Experimental results also show that the product anisotropy parameters are $\beta_2 > 0$ and $\beta_4 \sim 0$. The latter indicates that the intermediate state reached by the first one photon excitation has a quite long lifetime, while the former suggests the molecules undergo a parallel transition from the intermediate state to the final state upon the second photon excitation and then experience a fast dissociation process. Combined with previous studies, we propose a possible dissociation mechanism: after absorbing two photons in the range of 290.10–336.88 nm, the CS₂ molecule may undergo a sequential transition ${}^{1}A_{1}({}^{1}\Sigma_{\sigma}^{+}) \leftarrow 1{}^{1}B_{2}({}^{1}\Delta_{u})/{}^{1}A_{2}({}^{1}\Delta_{u}) \leftarrow X^{1}\Sigma_{\sigma}^{+}$, then directly dissociate or couple to other electronic states and dissociate.

Published under an exclusive license by AIP Publishing. https://doi.org/10.1063/5.0283135

INTRODUCTION

Carbon disulfide (CS2) is an important molecule in astrophysical media, the Earth's atmosphere, biological media, organic chemistry (as a building block), and industry as a chemical nonpolar solvent.¹ As a typical linear triatomic molecule, CS₂ possesses 16 valence electrons, the same as N2O, CO2, OCS, and ICN. In addition, CS₂ serves as a prototype molecular system for understanding the evolution process of wave packets on complex potentials, such as in the vicinity of conical intersections between potential energy

surfaces (PESs). Therefore, photodissociation dynamics and spectroscopy of CS₂ have been extensively investigated theoretically² and experimentally $^{8-15}$ in the last several decades.

The absorption spectrum of CS₂ between 100 and 410 nm shows many absorption bands and contains a wealth of resolved rovibrational structure. Jungen et al. 13 analyzed the absorption spectrum in the region of 290-370 nm. McGlynn and co-workers¹⁵ measured the photoabsorption spectrum and fluorescence cross sections of CS_2 in the regions of 188.2–213 and 287.5–339.5 nm. In the region of 290-410 nm, many of the structures have now been assigned

in terms of excitations to the so-called R, S, U, V, and T states (bent valence states), arising as a result of the electronic promotion $2\pi_g \to 3\pi_u$. Sunanda $\it et~al.^9$ recorded the photoabsorption spectrum of CS_2 in the region of 105–225.4 nm. The richly structured spectrum of CS_2 consists of both valence and Rydberg transitions overlapping each other within a few regions. These electronic states are assigned to the singlet or triplet states, which originate from $\{2\pi_g \to 3\pi_u, \, 7\sigma_g, \, 8\sigma_g, \, 6\sigma_u, \, 4\pi_u, \, 3\pi_g, \, 9\sigma_g\}, \, \{2\pi_u \to 3\pi_u, \, 7\sigma_g\},$ and $\{5\sigma_u \to 3\pi_u\}.$

The dissociation dynamics of CS₂ molecules are sensitive to the wavelength of photolysis. Previous studies showed that there are seven energetically accessible fragment channels from CS₂ photodissociation following optical excitation from the ultraviolet to vacuum ultraviolet region,

$$CS_2(^{1}\Sigma_g^{+}) + h\nu \rightarrow S(^{3}P) + CS(X^{1}\Sigma^{+}), \tag{1}$$

$$\to S(^1D) + CS(X^1\Sigma^+), \tag{2}$$

$$\to S(^1S) + CS(X^1\Sigma^+), \tag{3}$$

$$\rightarrow S(^{3}P) + CS(a^{3}\Pi), \tag{4}$$

$$\rightarrow C(^{3}P) + S_{2}(X^{3}\Sigma_{g}^{-}), \tag{5}$$

$$\rightarrow C(^{3}P) + S_{2}(a^{1}\Delta_{g}), \tag{6}$$

$$\rightarrow C(^{3}P) + S_{2}(b^{1}\Sigma_{g}^{+}). \tag{7}$$

A great deal of photodissociation studies of CS2 have been performed in the 185-230 nm region, which is related to channels (1) and (2). This absorption band has been attributed to a parallel electronic transition from the linear $X(^{1}\Sigma_{q}^{+})$ ground state to a singlet excited state. Conventionally, this singlet excited state is labeled as ${}^{1}\Sigma_{u}^{+}$ within the $D_{\infty h}$ symmetry and correlates with ${}^{1}B_{2}$ symmetry as the CS₂ molecule bends and descends to $C_{2\nu}$ symmetry. To reflect this, the singlet excited state is usually denoted as $^{1}B_{2}(^{1}\Sigma_{u}^{+})$. Yang et al. 6 studied the dissociation dynamics of CS₂ under collision-free conditions at 193.3 nm. They observed both the $S(^{1}D)$ and $S(^{3}P)$ atoms. The initially populated $^{1}B_{2}(^{1}\Sigma_{u}^{+})$ excited state may decay to form either the $S(^1D) + \overline{CS}(X^1\Sigma^+)$ channel or the $S(^3P)$ + $CS(X^1\Sigma^+)$ channel; the latter has been attributed to spin-orbit coupling mediating a crossing to the dissociative ${}^3\Pi_{\rm g}$ triplet electronic state. The ${}^{1}B_{2}({}^{1}\Sigma_{u}^{+})$ excited state decay dynamics were reported by Townsend and co-workers¹² in the region of 200 nm. They found that the dissociation dynamics of CS₂ reveals a biexponential modeling: a rapid decay pathway (τ < 50 fs) and a longer lived channel ($\tau \sim 350-650$ fs). The branching ratio of $S(^3P)/S(^1D)$, ranging from 0.25 to 6.0, has been reported by many experimental groups. By using the vacuum ultraviolet laser-induced fluorescence (LIF) spectroscopy of S atoms, Waller and co-workers¹⁷ concluded that the branching ratio of $S(^{3}P)/S(^{1}D)$ is 2.8 ± 0.3 , and Ng and co-workers¹⁸ confirmed this result by using the time-offlight photofragment translational spectroscopy. Subsequently, two independent measurements involving the velocity map ion imaging technique have reported the branching ratios of 1.5 \pm 0.4 by Kitopoulos *et al.*¹⁹ and 1.6 \pm 0.3 by Xu *et al.*²⁰ at the photolysis wavelength of 193 nm.

Moving to shorter wavelengths, the channels (3)-(7) gradually open up and become increasingly important. Black and coworkers²¹ studied the dissociation dynamics of CS₂ over the range 105-210 nm. They found that the quantum yield of $S(^1S)$ production is <0.1 throughout this region, and high yields of $CS(a^3\Phi)$ are produced between 125 and 140 nm. More recently, Li and co-workers²² reported the direct experimental evidence for the C(³P) product channels (5)-(7) from CS₂ photodissociation by using the velocity map ion imaging technique with one-photon vacuum ultraviolet (125-145 nm) and two-photon ultraviolet (300-320 nm) excitations. The very weak anisotropic angular distributions of photoproducts indicated relatively slow dissociation processes. They proposed a possible dissociation mechanism involving molecular isomerization of CS₂ to linear-CSS from the electronically excited ${}^{1}B_{2}(2^{1}\Sigma^{+})$ state via vibronic coupling with the ¹Π state, followed by an avoided crossing with the ground state surface.

In addition, two-photon photodissociation of CS2 is also one of the research focuses. By using mass-selected resonance-enhanced multiphoton ionization (REMPI) spectroscopy, Hardwick et al.²³ studied two-photon dissociation of CS₂ in the region of 280–330 nm. On the basis of their experimental observations, they were able to identify the fragments CS in its $a^3\Pi$ state, atomic carbon in its 3P , ¹D, and ¹S electronic states, and sulfur in its ³P, ¹D, and ¹S electronic states. The results indicated that little of the available energy from CS₂ photodissociation is deposited as product translational energy, but rather that most is taken up by the internal degrees of freedom of the photoproducts. Kawasaki and co-workers^{24,25} investigated the two-photon dissociation of CS₂ in the range of 288-310 nm by measuring the speed and angular distributions of the $S(^3P)$ and $S(^1D)$ photofragments. By analyzing the photofragment angular distributions, they found that after the first one-photon absorption, the intermediate ¹B₂ electronic state has a quite long lifetime compared to the laser pulse, so the angular distributions of photofragments would be determined solely by the second transition from the intermediate ¹B₂ electronic state to the higher dissociative electronic state, and the coherence between the first and the second photons should not be significant. On the basis of their results, they suggested that CS₂ may undergo a sequential transition ${}^{1}A_{1} \leftarrow {}^{1}B_{2} \leftarrow X^{1}A_{1}$, then directly dissociate or couple to other electronic states and dissociate. Sapers and Donaldson^{26,27} detected the $CS(X^1\Sigma^+)$ fragment from CS₂ two-photon dissociation at 308 nm by using the LIF technique. They determined the vibrational distribution of the $CS(X^1\Sigma^+)$ products and found that the distribution is inverted and bimodal but rather narrow. By using the ion imaging technique, Samartzis and Kitsopoulos¹¹ investigated two-photon dissociation of CS₂ at 289.9, 308.2, 310.1, and 310.9 nm. From the S atom product translational energy distribution, they distinguished the $S(^{3}P) + CS(X^{1}\Sigma^{+})$ channel and the $S(^{3}P) + CS(a^{3}\Pi)$ channel with a branching ratio $S(^{3}P)$ $+ CS(a^3\Pi)/S(^3P) + CS(X^1\Sigma^+) = 0.22 \pm 0.05$ at 308.2 nm. Based on the angular distributions of photofragments, they concluded that the excited electronic states involved in the two-photon dissociation of CS₂ are the Rydberg states with predissociation lifetimes estimated around 1 ps. More recently, by using the velocity map ion imaging technique, Li and co-workers¹⁴ investigated photodissociation

dynamics of CS₂ through two-photon excitation in the range of 303–315 nm. From the ion images of the S(³P) and S(¹D) photoproducts, the product channels (1), (2), and (4) were identified. At photolysis wavelength 303.878 nm, the branching ratios of S(³P) + CS(a³Π)/S(³P) + CS(X¹Σ⁺) were determined to be 0.05 \pm 0.02, 0.17 \pm 0.04, and 0.26 \pm 0.05 for the three spin–orbit states S (³P₀), S (³P₁), and S (³P₂), respectively, which implied a strong spin–orbit coupling in the dissociation process. Based on the angular distributions of photoproducts, they suggested that CS₂ may undergo a sequential transition $^1B_2(2^1\Sigma^+)\leftarrow 1^1B_2(^1\Delta_u)\leftarrow X^1\Sigma_g^+$, with the intermediate electronic state $1^1B_2(^1\Delta_u)$ having a long lifetime, followed by nonadiabatic and spin–orbit couplings to other electronic states and then dissociation.

To date, the dynamical information of the $S(^1S)$ product channel (3) from CS_2 photodissociation is very limited. In this work, by using the time-sliced velocity map ion imaging technique, we investigated the $S(^1S) + CS(X^1\Sigma^+)$ channel through two-photon excitation of CS_2 in the range of 290.10–336.88 nm. By measuring the $S(^1S)$ ion image, the $CS(X^1\Sigma^+)$ internal state populations and the angular distributions are obtained. The rovibrational states of the CS products are partially resolved in the experimental images. The new results should be helpful in revealing the two-photon dissociation mechanism of CS_2 in the excited states.

EXPERIMENT

The CS₂ photodissociation experiment was carried out in a sliced velocity map ion imaging apparatus. The experimental methodology and procedures in this study are similar to those described in previous publications.^{28–32} In brief, the pulsed supersonic molecular beam was generated by expanding a gas mixture (0.02% CS2 in Ar) into the source chamber via a pulsed valve with a 0.5 mm orifice, where it was skimmed before entering and propagating along the center axis of the ion optics assembly (IOA, 23-plate ion optics) mounted in the reaction chamber. The collimated beam passed through a 2 mm hole in the first electrode and propagated along the center axis of the IOA toward the center of the front face of the detector. The molecular beam was orthogonal to the counterpropagating photolysis and probe laser beams between the second and third plates of the IOA. The dissociation of the CS2 molecule proceeded via sequential two-photon absorption in the range of 290.10-336.88 nm. After a delay time of 15 ns, the S(1S) fragments were state-selectively ionized by (2 + 1) REMPI at the wavelength of 290.10 nm. The photolysis and probe lasers were generated by doubling the outputs of two tunable dye lasers, which were pumped by the second harmonic (532 nm) of their respective Nd:YAG lasers with a 10 Hz repetition rate. In the experiment, the polarization directions of the two laser beams were set to be parallel to the detector plane.

Then the resulting S⁺ ions were accelerated through the remainder of the IOA and passed through a 765 mm long field-free region before impacting a dual microchannel plate (MCP) coupled with a P47 phosphor screen. The instantaneous images on the phosphor screen were captured and recorded by a charge-coupled device (CCD) camera. The time controlled system consisted of two multichannel digital delay generators (DG645, SRS).

RESULTS AND DISCUSSION

Figure 1 displays the absorption spectrum of CS₂ in the wavelength range of 281-351 nm. This absorption spectrum assigned by Kleman as the V system³³ extends from the 1 V band at 332.2 nm to the 48 V band at 295.3 nm. The V band extends to ~290 nm, but the assignment is lacking at wavelengths shorter than 295.3 nm. Meanwhile, the absorption spectrum in the range of 334-350 nm has been assigned by Jungen et al. 13 as the T system. They concluded that the V band corresponds to the ${}^{1}B_{2}({}^{1}\Delta_{u}) \leftarrow {}^{1}\Sigma_{g}^{+}$ transition and the T band corresponds to the ${}^{1}A_{2}({}^{1}\Delta_{u}) \leftarrow {}^{1}\Sigma_{g}^{+}$ transition. They further assigned the vibrational structures of the V band as involving the bending vibration transition $v_2'-v_2''$. However, the vibrational assignments of the T band are still unclear. To investigate the $S(^{1}S) + CS(X^{1}\Sigma^{+})$ channel following the two-photon photoexcitation of CS₂, the time-sliced images of the S(¹S) photoproducts were measured at selected photolysis wavelengths marked by red arrows in Fig. 1 using the above-mentioned method. Figure 2 displays the raw images of the S(1S) photoproducts from CS₂ two-photon photo dissociation at 290.10, 299.44, 307.35, and 321.48 nm, respectively. Each image was obtained by accumulating the S⁺ signals over 30 000 laser shots with background subtraction. The red vertical double arrow shown in Fig. 2 indicates the polarization direction of the photolysis laser. It is found that each S(1S) image displays a series of well-resolved concentric rings with different intensities, and these structures are assigned to the rovibrational states of the partner CS product in the $S(^{1}S) + CS(X^{1}\Sigma^{+})$ binary dissociation process. In addition, these concentric rings exhibit a distinct anisotropic angular distribution.

Based on the measured images, the velocity distributions of the $S(^1S)$ photoproducts could be extracted by integrating the signals in the images over the entire angular range. On the basis of these velocity distributions, the total kinetic energy release (TKER) spectra in

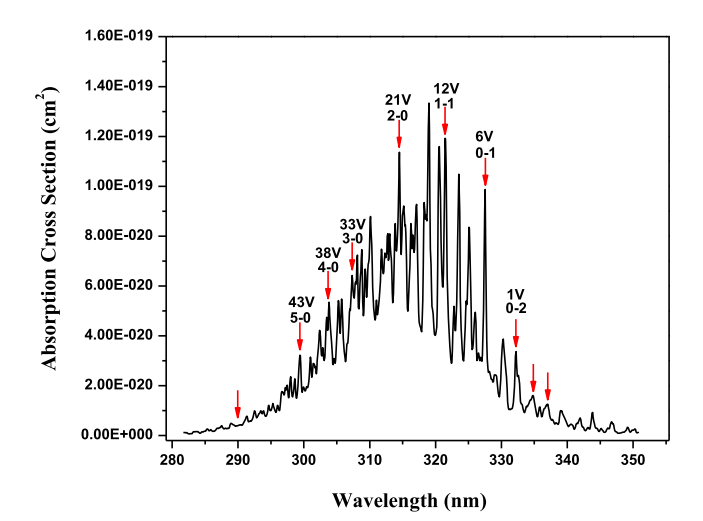


FIG. 1. Absorption spectrum of CS $_2$ in the wavelength range of 281–351 nm (the data were obtained from www.uv-vis-spectral-atlas-mainz.org). The positions of the photolysis excitation wavelengths used in this work are indicated by the red downward pointing arrows. The corresponding vibrational assignments are involved in the bending vibration $v_2'-v_2''$.

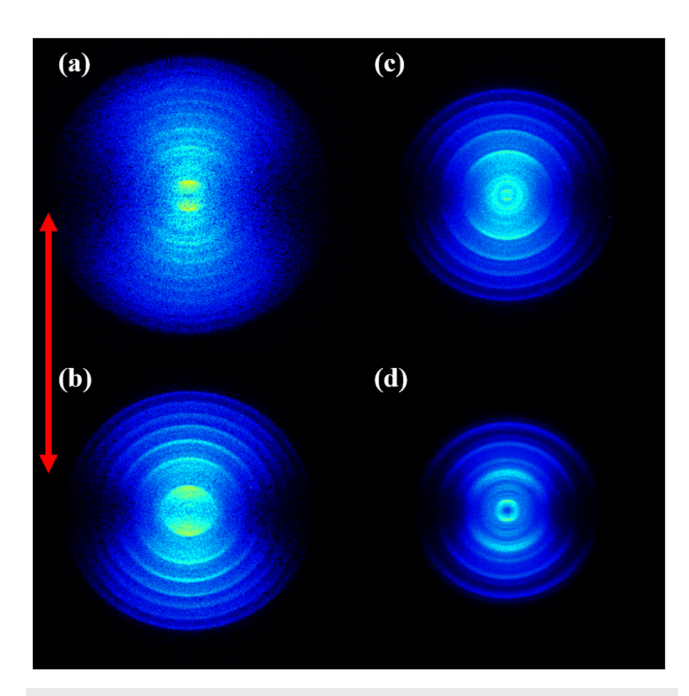


FIG. 2. Raw image of the S(1S) product from the two-photon dissociation of CS₂ at (a) 290.10 nm, (b) 299.44 nm, (c) 307.35 nm, and (d) 321.48 nm. The double arrow indicates the polarization direction of the photolysis laser.

the center-of-mass frame are acquired according to the conservation of energy and linear momentum. Figure 3 displays the resulting TKER spectra from two-photon dissociation of CS₂ at the photolysis wavelengths mentioned earlier. It is clear that these TKER spectra comprise of a series of well resolved peaks extending to the energy limit of the available energy.

Since the S(1S) atomic photoproduct possesses only the electronic energy, the observed peaks in the TKER spectra correspond directly to the rovibrational states of the CS co-product according to the following equation:

$$E_{hv} + E_{int}(CS_2) - D_0 = E_T + E_{int}(S) + E_{int}(CS),$$
 (8)

where E_{hv} denotes the two-photon energy of the photolysis laser, D_0 represents the dissociation threshold energy of the $S(^{1}S) + CS(X^{1}\Sigma^{+})$ channel, E_T is the photoproduct total kinetic energy, E_{int}(CS₂) and Eint(CS) are the internal energies of the CS2 and CS products, respectively, and E_{int}(S) is the energy difference between the S(¹S) electronic state and the ground state $S(^{3}P_{2})$.

As marked in Fig. 3, we have assigned the peaks to the formation of $CS(X^1\Sigma^+)$ vibrational states. It is clear that the onsets of the TKER spectra are in excellent agreement with the known dissociation threshold of $S(^1S) + CS(X^1\Sigma^+)$ channel, confirming that the CS photoproducts are produced in correlation with the S(1S) atomic products. As can be seen in Fig. 3, the CS products are obviously highly vibrationally inverted and can populate up to the energy limit of the available energy. It is noted that the $CS(X^1\Sigma^+)$ photoproducts show quite similar distributions at all four

photolysis wavelengths, suggesting a similar dissociation mechanism in this wavelength region. Furthermore, a closer analysis reveals that most of the $CS(X^1\Sigma^+)$ vibrational states consist of two partially resolved peaks, which correspond to the low and high rotationally excited CS photoproducts. This phenomenon is similar to our previous results of CO₂ photodissociation around 108 nm.³⁴ The complex profile for single vibrational excitation indicates that the $CS(X^1\Sigma^+)$ photoproducts have nonstatistical rotational excitation.

Proceeding to longer wavelengths, Fig. 4 displays the raw images of the S(1S) photoproducts of CS₂ following two-photon photodissociation at 327.53, 332.23, and 336.88 nm. Obviously, as the photoexcitation energy decreases, the ring sizes of the S(1S) images become smaller, and the correlated CS vibrational state distribution shifts to a lower vibrational state. Figure 5 displays the resulting TKER spectra derived from the speed distributions in Fig. 4. The rovibrational state assignments of the $CS(X^1\Sigma^+)$ photofragments from photodissociation of CS₂ are also marked in Fig. 5. It can be seen that a clear peak appears beyond the threshold of the energetically allowed $S(^{1}S) + CS(X^{1}\Sigma^{+})$ channel in the TKER spectra at 332.23 and 336.88 nm. Since the extension of these signals to the higher kinetic energy is in excellent accordance with the energy of the CS2 bending vibrational mode, it can be assigned to the rovibrational levels of the $CS(X^1\Sigma^+)$ photoproducts from photo dissociation of $CS_2(\nu_2 = 1)$. Similar phenomena originating from the vibrationally excited parent molecule have also been obviously observed in CO₂ photodissociation.³⁵ Furthermore, we found that as the wavelength gradually increases from 327.53 to 336.88 nm, the proportion of the $S(^1S) + CS(X^1\Sigma^+)$ photoproducts from the vibrationally excited CS2 molecule gradually increases. This means the bending vibrational mode of the parent molecule is beneficial for the photolysis of CS2. The result is consistent with the assignment of the absorption spectrum of CS₂. 13 Based on the structure analysis of the gas-phase absorption spectrum of CS₂ in the region 290-330 nm (V system), Jungen et al. 13 pointed out that the absorption spectrum in this region corresponds to the ${}^{1}B_{2}({}^{1}\Delta_{u}) \leftarrow {}^{1}\Sigma_{g}^{+}$ transition, where the ¹B₂ state correlates with the upper Renner-Teller component of the $\pi \to \pi^{*1} \Delta_u$ state of the linear molecule, while the absorption spectrum in the range of 334-350 nm (T system) corresponds to the lower Renner-Teller component ${}^{1}A_{2}({}^{1}\Delta_{u}) \leftarrow {}^{1}\Sigma_{g}^{+}$ transition. These consist of a progression of the vibronic Δ - Δ bands and a weaker progression of the Π - Π bands. In addition, the bands of both V and T systems are severely perturbed. Compared with the V system, the absorption spectrum of the T system is vibrationally hot. The product's total translational energy release spectra at 332.23 and 336.88 nm indeed display the hot band feature as shown in Fig. 5. Therefore, the $S(^1S) + CS(X^1\Sigma^+)$ dissociation channel of CS_2 at 332.23 and 336.88 nm may originate from the lower Renner-Teller component ${}^{1}A_{2}({}^{1}\Delta_{u}) \leftarrow {}^{1}\Sigma_{g}^{+}$ transition of the T system.

In order to obtain more detailed information on the rovibrational distribution of the CS co-products, a qualitative simulation of the TKER spectra was carried out. The simulation used a multipeak fitting method in which a group of Gaussian profiles (each peak corresponds to a rotational state of the CS products) was employed to fit one vibrational peak in the TKER spectra. As shown in Figs. 3 and 5, the red solid curve in each graph represents the global result of a multipeak fitting. The dashed green and cyan lines are the individual CS vibrational components originating from ground $CS_2(v_2 = 0)$, and the dashed purple lines in Figs. 5(b) and 5(c)

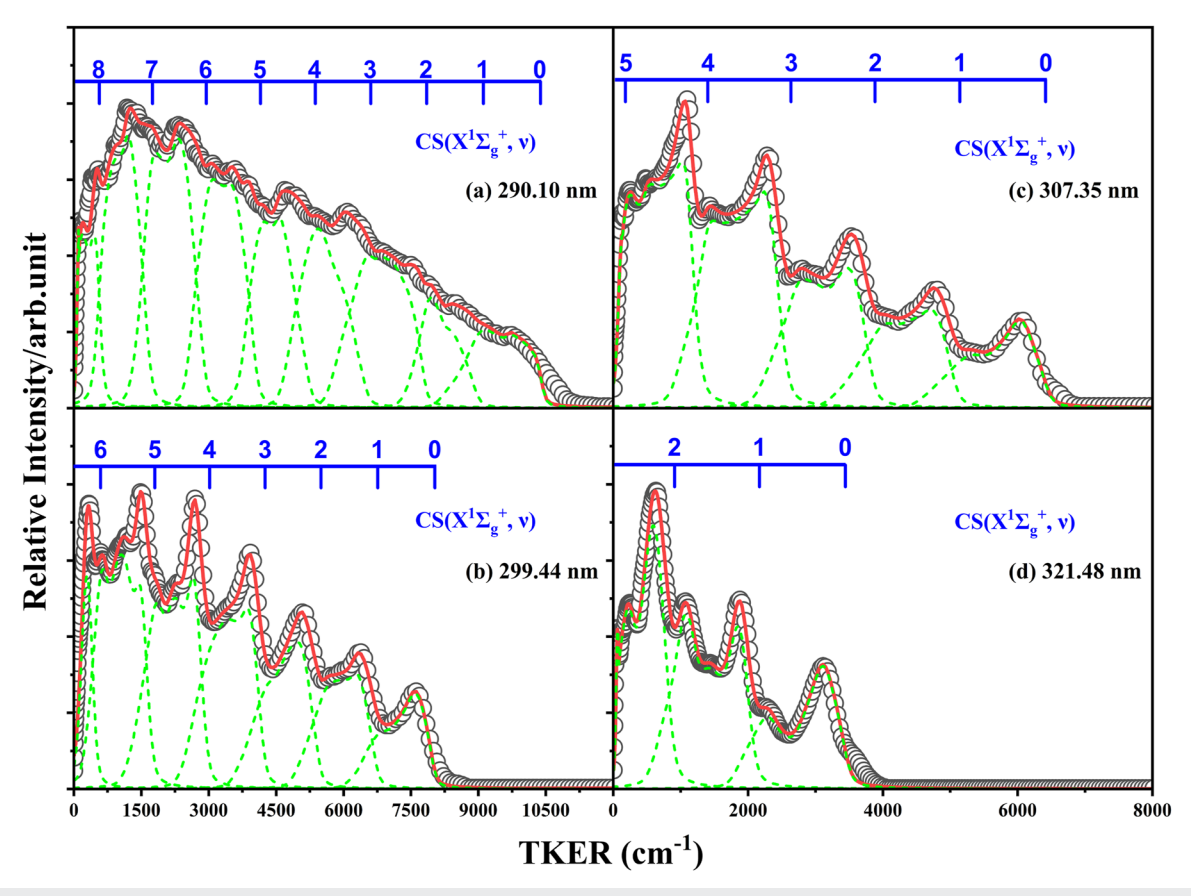


FIG. 3. Product total translational energy release spectra derived from the speed distributions in Fig. 2 for the $S(^1S) + CS(X^1\Sigma^+)$ channel. The red lines are the fitting results, and the dashed green lines are the individual CS vibrational components. The drop lines on each of the spectra, respectively, designate the vibrational levels of the CS(v|j) photoproducts from photodissociation of CS_2 .

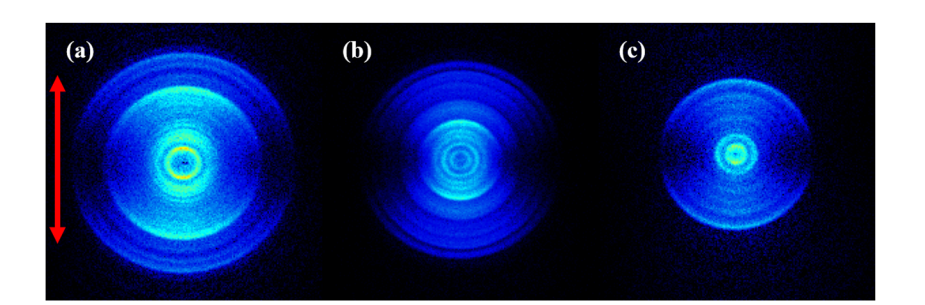


FIG. 4. Raw image of the $S(^1S)$ product from the two-photon dissociation of CS_2 at (a) 327.53 nm, (b) 332.23 nm, and (c) 336.88 nm. The double arrow indicates the polarization direction of the photolysis laser.

are the CS components originating from vibrationally excited CS_2 ($\nu_2=1$). The fitting process is complicated by the overlap of rotational levels associated with different vibrational states of the CS product, which can obscure the relative contributions of the different levels in the simulation. The rational assumption is that the rotational population distributions associated with each vibrational state vary relatively smoothly with j. As can be seen in Fig. 5, the CS products are populated in rotational states up to the limit of available energy, which is similar to our previous results of CO_2 photodissociation at 157 nm.³⁵ The high rotationally excited CS

products imply that a strong torque is exerted on the CS products during the process of dissociation, and the photodissociation of CS₂ in this region should take place in a bent dissociative state. Similar to CO₂, the anomalous rotational structure can be interpreted as the rotational rainbow effect. ^{36,37} In addition, as shown in Fig. 5(a), the CS($\nu = 0$) rotational distributions can be described by the sum of two broad distributions at low-j and high-j values, and the low-j profile displays three partially resolved peaks. Normally, for this type of triatomic molecule, the low rotationally excited photoproducts are likely produced from a nearly linear dissociating molecule, while the

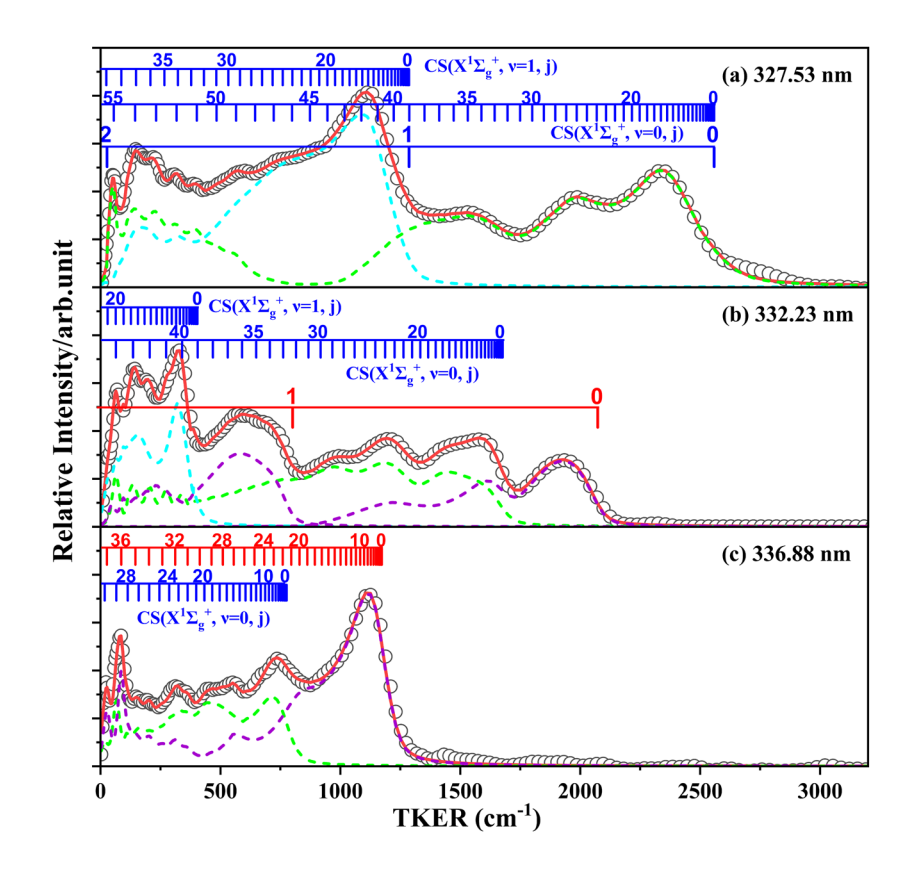


FIG. 5. Product total translational energy release spectra derived from the speed distributions in Fig. 4 for the S(1S) + $CS(X^1\Sigma^+)$ channel. The red lines are the fitting results. The dashed green and cyan lines are the individual CS vibrational components originating from the ground state $CS_2(v_2 = 0)$, and the dashed purple lines in (b) and (c) are the CS components arising from the vibrationally excited $CS_2(v_2 = 1)$. The drop lines on each of the spectra, respectively, designate the rovibrational levels of the CS(v|j) photoproducts from photo dissociation of $CS_2(v_2 = 0)$ (blue) and $CS_2(v_2 = 1)$ (red).

high rotationally excited photoproducts are likely produced from a more bent dissociating molecule.

Based on the fitting results, the contributions from vibrationally excited $CS_2(v_2 = 1)$ photodissociation at 332.23 and 336.88 nm are found to be ~41% and 65%, respectively. The uncertainty is large due to severe overlapping of components from $CS_2(v_2 = 1)$ and $CS_2(v_2 = 0)$ in the low translational energy region. Figure 6 shows the relative vibrational state populations of the CS photoproducts. It is interesting that the CS vibrational state distributions share similar profiles with a peak at ν_{max} – 1 (ν_{max} represents the maximum vibrational quantum number allowed by the available energy) except for 290.10 nm ($\nu_{\rm max}$ – 2). The similar distributions usually imply a similar dissociation mechanism in this wavelength region. Such high vibrational excited CS photoproducts may be due to the couplings between the upper electronic states, such as vibronic coupling. In the dissociation process, the C-S bond should elongate; when one C-S bond breaks, the other will cause the formation of highly vibrationally excited CS photoproducts.

The product spatial angular distribution was also obtained by integrating the images over the relevant radius region. The results were then fitted by using the relation displayed in the equation

$$I(\theta) = \sigma [1 + \beta_2 P_2(\cos \theta) + \beta_4 P_4(\cos \theta)], \tag{9}$$

where σ is the product translational energy distribution and θ is the scattering angle between the direction of the recoil velocity of the atomic sulfur products and the polarization axis of the linearly

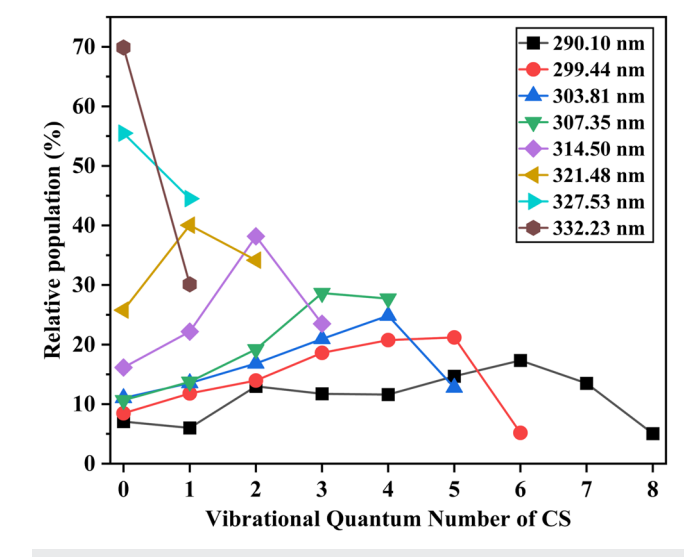


FIG. 6. Vibrational state distribution of the $CS(X^1\Sigma^+)$ photoproducts from the two-photon dissociation of CS_2 in the wavelength range of 290.10–332.23 nm.

polarized photolysis laser. β_2 and β_4 are the anisotropy parameters that depend on the photodissociation rates for the formation of specific photofragments and the geometry of the excited molecule, and P_2 and P_4 are the second- and fourth-order Legendre polynomials.

TABLE I. Average anisotropy parameter values derived from simulations of differential cross sections for S(¹S) photoproducts.

Wavelength (nm)	eta_2	eta_4
290.100	0.637	0.010
299.444	0.590	-0.008
303.810	0.548	0.005
307.348	0.475	0.001
314.500	0.543	-0.046
321.480	0.572	-0.035
327.530	0.584	-0.005
332.230	0.543	-0.010
334.760	0.609	-0.008
336.880	0.491	-0.005

The overall anisotropy parameters were determined by fitting the angular distributions in Figs. 2 and 4. Table I lists the overall anisotropy parameters of S(1S) photoproducts in the wavelength range of 290.10-336.88 nm. The averaged β_2 values over the product translational energy distribution are all around 0.55 for S(1S) photoproducts at the ten photolysis wavelengths, while the averaged β_4 values are all close to zero. The contribution of the P₄ term is quite small in this two-photon dissociation of CS₂, similar to that observed by Kawasaki and co-workers,²⁵ in which the β_4 values could be ignored. This result implies that the photodissociation of CS2 is due to the two-photon absorption via the real intermediate state ${}^{1}B_{2}({}^{1}\Delta_{u})$ or ${}^{1}A_{2}({}^{1}\Delta_{u})$. The anisotropy parameter values observed in this work are in fair agreement with Li's results. 14 According to the previous results, ^{13,38} the absorption band of CS₂ in the range of 290–330 nm corresponds to the ${}^{1}B_{2}({}^{1}\Delta_{u}) \leftarrow {}^{1}\Sigma_{\sigma}^{+}$ transition, and this intermediate ${}^{1}B_{2}({}^{1}\Delta_{u})$ state is bent with an $\angle S-C-S$ angle around 131°. The intermediate ${}^{1}B_{2}({}^{1}\Delta_{u})$ state has a quite long lifetime compared with the laser pulse duration; therefore, the angular distribution is determined solely by the second transition from the intermediate ${}^{1}B_{2}({}^{1}\Delta_{u})$ state to the higher final state, and the correlation between the first and the second photons would not be significant. Based on the angular distributions of photoproducts in the wavelength range of 332.23-336.88 nm (T system), which is similar to that from the ${}^{1}B_{2}({}^{1}\Delta_{u})$ state, the intermediate state ${}^{1}A_{2}({}^{1}\Delta_{u})$ should also have an equally long lifetime.

In order to obtain more detailed anisotropy parameters, Fig. 7 depicts the state dependent β_2 value for $CS(\bar{X}^{\bar{1}}\bar{\Sigma}^{\bar{+}})$ photoproducts from two-photon dissociation of CS2 in the wavelength range of 290.10–327.53 nm. These vibration state dependent β_2 values reveal a roughly decreasing trend with increasing $CS(X^1\Sigma^+)$ vibrational quantum number. This decreasing trend may be partially due to the weak signal compared to the roughly isotropic background. Similar to CO2, the decreasing trend suggests that the high vibrational CS products come from the dissociating CS₂ molecule with a geometry slightly more bent than the low vibrational CS products. The transition dipole for excitation to the upper state will lie in the plane of the bent CS₂ and nearly parallel to the C-S bond for small bending angles. For the prompt dissociation, the in-plane transition to the upper state is expected to be nearly parallel for small bending angles of the CS₂ parent and would result in a large β_2 value close to 2. However, if the parent molecule bends before dissociation, the

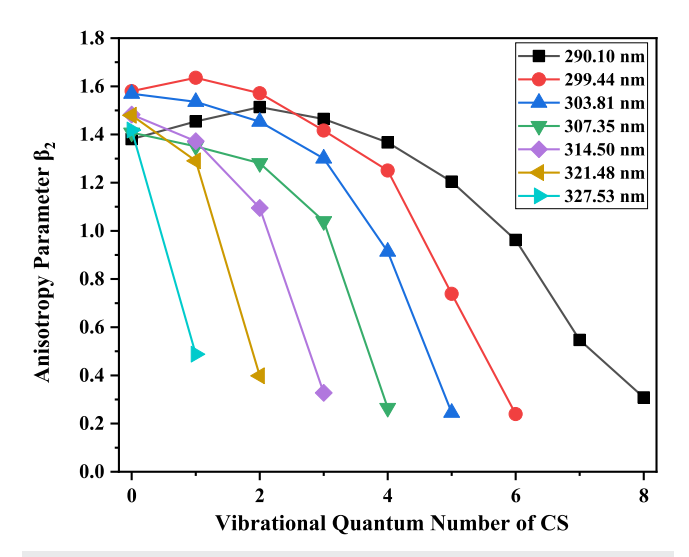


FIG. 7. Vibrational state dependence of the β_2 value for CS(X¹ Σ^+) photoproducts from the two-photon dissociation of CS₂ in the wavelength range of 290.10–327.53 nm.

fragment velocity vector will no longer be as highly aligned with the transition dipole, and the β_2 value will be reduced. Therefore, the reduced β_2 value for high vibrational excited states of CS may be due to some bending as CS₂ dissociates.

The β_2 values for the CS(X¹ Σ^+) photoproducts from the vibrationally excited CS₂ (the component with the translational energy being higher than the threshold energy of the S(¹S) + CS(X¹ Σ^+) channel in the TKER spectra) are all around 1.6 in the wavelength range of 332.23–336.88 nm, and the β_4 values are close to zero. Due to the similarity of angular distributions for CS products from the ground and excited CS₂ molecules, the dissociation mechanism should be similar, which means the dissociation of CS₂ in the excited states is prompt, with the dissociation lifetimes being shorter than the rotational periods of excited CS₂ molecules.

There is a high density of excited electronic states located in the two-photon energy range of 7.36-8.55 eV (290.10–336.88 nm), which could cause strong mixing of the upper electronic state by vibronic coupling, spin–orbit interactions, and so on, resulting in complex electronic and rovibrational spectra. It is obvious that the dissociation mechanism of the CS₂ molecule is quite complex. Theoretical calculations of the PESs are significant for understanding the photodissociation mechanism of CS₂.

Recently, Trabelsi *et al.*⁷ have constructed the 3D PESs of the three isomers of CS₂, i.e., linear SCS, bent *cyc*-CS₂, and linear CSS, by *ab initio* calculations. The evolution of the lowest-lying singlet and triplet electronic states along the S–S and C–S stretching coordinates and along the bending angle was mapped. Their results revealed that after absorbing a photon with $hv \ge 7.08$ eV (174 nm), the transition dipole moment of the second ${}^{1}B_{2}({}^{1}\Sigma^{+})$ (i.e., ${}^{2}L^{2}$) state $\leftarrow X^{1}\Sigma_{g}^{+}$ is relatively large. Therefore, the ${}^{1}B_{2}(2^{1}\Sigma^{+})$ state of CS₂ can be effectively populated and should play a major role in the isomerization and photodissociation processes occurring at these energies. As shown in Figs. 3 and 5(a) in Ref. 7, the potential of the ${}^{1}B_{2}(2\Sigma^{+})$ state is shallow and flat along the C–S distance and bending angle.

The wave packet would experience large parts of this potential and evolve to the $S(^1S) + CS(X^1\Sigma^+)$ photoproducts when the excitation energy is higher than the $S(^1S) + CS(X^1\Sigma^+)$ asymptote energy. Based on this calculation and the experimentally observed angular distributions of photoproducts, Li and co-workers¹⁴ suggested that after absorbing two photons in the range of 303-315 nm, CS₂ could undergo a sequential transition ${}^{1}B_{2}(2^{\bar{1}}\Sigma^{+}) \leftarrow 1{}^{1}B_{2}({}^{1}\Delta_{u}) \leftarrow X^{1}\Sigma_{g}^{+}$. The ${}^{1}B_{2}(2^{1}\Sigma^{+})$ state has been regarded as a ${}^{1}B_{2}({}^{1}\Sigma_{u}^{+})$ state with odd parity by Trabelsi et al.,7 and the transition dipole moment of the SCS $^{1}B_{2}(2\Sigma_{u}^{+}) \leftarrow X^{1}\Sigma_{g}^{+}$ transition is relatively large after absorbing a photon with $hv \ge 7.08$ eV (174 nm). However, after absorbing two photons, the ${}^{1}B_{2}(2^{1}\Sigma_{u}^{+})$ state of CS₂ may not be necessarily effectively populated, and the upper electronic state of CS2 should usually have an even parity. The transition rules of two-photon excitation are different from those of single photon excitation. Although the two-photon electronic transition to the u state is vibrationally allowed through the bending mode of CS2, the intensity should be extremely weak. Therefore, after absorbing the second photon from the intermediate ${}^{1}B_{2}({}^{1}\Delta_{u})$ state, the upper electronic state of CS₂ should usually have an even parity. The excited electronic states $^{1}\Sigma_{g}^{+},\,^{1}\Pi_{g},$ and $^{1}\Delta_{g}$ can serve as possible candidates.

After absorbing two photons in the range of 290.10-336.88 nm, the CS₂ molecule can be formed in the excited 3d Rydberg states. By promoting a π_g electron to the 3d orbital Rydberg states, the excited electronic states ${}^{1}\Sigma_{g}^{+}$, ${}^{1}\Pi_{g}$, and ${}^{1}\Delta_{g}$, which correlate to the product energy states, can be formed.⁴¹ CS₂ reaches these excited states by sequential absorption of two photons via the real intermediate ${}^{1}B_{2}({}^{1}\Delta_{u})$ or ${}^{1}A_{2}({}^{1}\Delta_{u})$ state. Kawasaki and co-workers²⁵ proposed that if the upper state retains the structure of the intermediate ¹B₂ state ($\angle S$ -C-S angle is around 131°), only the ${}^{1}A_{1} \leftarrow {}^{1}B_{2} \leftarrow X^{1}A_{1}$ transition can give the positive β_2 value. In addition, Venkitachalam and Rao⁴¹ proposed that after absorbing two photons in the region 285–305 nm, the CS_2 molecule in the excited $^1\Sigma_g^+$ state can give rise to the products $S(^1S) + CS(X^1\Sigma^+)$. Based on the above-mentioned results and our positive anisotropy parameters, we propose a possible dissociation mechanism for the $S(^1S) + CS(X^1\Sigma^+)$ channel. After absorbing two photons in the range of 290.10-336.88 nm, the CS_2 molecule may undergo a sequential transition ${}^1A_1({}^1\Sigma_g^+)$ $\leftarrow 1^1 B_2(^1 \Delta_u) \leftarrow X^1 \Sigma_g^+ \text{ for the V system and } ^1 A_1(^1 \Sigma_g^+) \leftarrow ^1 A_2(^1 \Delta_u^-)$ $\leftarrow X^1\Sigma_g^+$ for the T system, then directly dissociate or couple to other electronic states and dissociate. Similarly, the excided CS₂ molecule may also couple to the $^1B_2(2^1\Sigma^+)$ state and evolve to the $S(^1S)$ + $CS(X^1\Sigma^+)$ products. However, due to the lack of highly accurate PESs of the excited electronic states, the detailed dissociation process on the PESs is not clear. To unambiguously illustrate the dissociation characteristics for the $S(^1S) + CS(X^1\Sigma^+)$ channel observed in this work, further theoretical calculations are required. Nevertheless, these new results obtained in this experiment should provide new insights into the two-photon dissociation mechanism for the $S(^{1}S) + CS(X^{1}\Sigma^{+})$ channel.

CONCLUSIONS

The $S(^1S)$ + $CS(X^1\Sigma^+)$ channel for the two-photon photodissociation of CS_2 was studied via the time-sliced velocity map ion imaging technique in the range of 290.10–336.88 nm. The atomic

sulfur fragment $S(^1S)$ was probed. The $CS(X^1\Sigma^+)$ product rovibrational state distributions and product angular distributions have been determined from the $S(^1S)$ images. By analyzing the photofragment translational energy distributions, we found that the CS vibrational state distributions share similar profiles with a peak at $\nu_{max}-1$ or $\nu_{max}-2$. A closer analysis reveals that most of the $CS(X^1\Sigma^+)$ vibrational states exhibit a bimodal or more complex rotational structure. On the basis of the experimental results, the $^1A_1(^1\Sigma_g^+)$ state should play a significant role in the two-photon photodissociation processes occurring at the excitation energies in this work. These new results should provide a sensitive testing ground for theoretical studies on the two-photon dissociation dynamics of CS_2 in the excited states.

ACKNOWLEDGMENTS

This work is supported by the National Natural Science Foundation of China (Grant Nos. 22241304, 22225303, 22403091, and 22173100), the Major Program of the National Natural Science Foundation of China (Grant No. 42494853), the Innovation Program for Quantum Science and Technology (Grant No. 2021ZD0303304), the Strategic Priority Research Program of the Chinese Academy of Sciences (Grant Nos. XDB0970000 and XDB0970200), and the Liaoning Revitalization Talents Program (Grant No. XLYC2402046), the Excellent Young Teacher Cultivation Project of the Education Department of Anhui Province (Grant No. YQZD20230590), the Natural Science Research Project of the Education Department of Anhui Province (Grant No. 2023AH050426), the Undergraduate Quality Engineering Project of Fuyang Normal University (Grant No. 2023JYXM0036), the Open Foundation of the State Key Laboratory of Molecular Reaction Dynamics in DICP, CAS (Grant Nos. SKLMRD-K202407, SKLMRD-K202513, and SKLMRD-K202505), the Excellent Research and Innovation Team of Functional Materials and Devices for Informatics of Anhui Higher Education Institute (Grant No. 2024AH010024), and the GuangDong Basic and Applied Basic Research Foundation (Grant No. 2025A1515012671). X.Y. also acknowledges the Guangdong Science and Technology Program (Grant Nos. 2019ZT08L455 and 2019JC01X091) and the Shenzhen Science and Technology Program (Grant No. ZDSYS20200421111001787).

AUTHOR DECLARATIONS

Conflict of Interest

The authors have no conflicts to disclose.

Author Contributions

Shuaikang Yang and Zhiguo Zhang contributed equally to this paper.

Shuaikang Yang: Data curation (equal); Formal analysis (equal); Funding acquisition (equal); Methodology (equal); Project administration (supporting); Validation (equal); Writing – original draft (equal); Writing – review & editing (supporting). **Zhiguo Zhang**:

Data curation (equal); Formal analysis (equal); Funding acquisition (equal); Methodology (equal); Project administration (equal); Validation (equal); Writing - original draft (equal); Writing review & editing (equal). Yongxin Dong: Data curation (equal); Formal analysis (equal); Methodology (equal). Zijie Luo: Data curation (equal); Formal analysis (equal); Methodology (equal). Wei Hua: Data curation (equal); Formal analysis (equal); Methodology (equal). Zhenxing Li: Data curation (equal); Formal analysis (equal); Funding acquisition (equal). Quan Shuai: Formal analysis (equal); Methodology (equal); Validation (equal). Xingan Wang: Formal analysis (equal); Methodology (equal); Supervision (equal); Writing - review & editing (equal). Kaijun Yuan: Data curation (equal); Formal analysis (equal); Funding acquisition (equal); Methodology (equal); Project administration (equal); Validation (equal); Writing - review & editing (equal). Xueming Yang: Formal analysis (supporting); Project administration (equal); Writing review & editing (equal).

DATA AVAILABILITY

The data that support the findings of this study are available from the corresponding authors upon reasonable request.

REFERENCES

- ¹ A. W. DeMartino, D. F. Zigler, J. M. Fukuto, and P. C. Ford, Chem. Soc. Rev. 46, 21 (2017).
- ²D. C. Tseng and R. D. Poshusta, J. Chem. Phys. **100**, 7481 (1994).
- ³Q. Zhang and P. H. Vaccaro, J. Phys. Chem. **99**, 1799 (1995).
- ⁴S. T. Brown, T. J. Van Huis, B. C. Hoffman, and H. F. Schaefer, Mol. Phys. **96**, 693 (1999).
- ⁵K. B. Wiberg, Y.-g. Wang, A. E. de Oliveira, S. A. Perera, and P. H. Vaccaro, J. Phys. Chem. A **109**, 466 (2005).
- ⁶E. Pradhan, J. L. Carreon-Macedo, J. E. Cuervo, M. Schroder, and A. Brown, J. Phys. Chem. A **117**, 6925 (2013).
- ⁷T. Trabelsi, M. M. Al-Mogren, M. Hochlaf, and J. S. Francisco, J. Chem. Phys. **149**, 064304 (2018).
- ⁸G. Brasen and W. V. Demtroder, J. Chem. Phys. 110, 11841 (1999).
- ⁹K. Sunanda, A. Shastri, A. K. Das, and B. N. Raja Sekhar, J. Quant. Spectrosc. Radiat. Transfer 151, 76 (2015).
- ¹⁰E. Dayan, E. Dervil, J. Loisel, J. P. Pinan-Lucarre, and G. Tarjus, Chem. Phys. 119, 107 (1988).
- ¹¹P. C. Samartzis and T. N. Kitsopoulos, J. Phys. Chem. A **101**, 5620 (1997).
- ¹²D. Townsend, H. Satzger, T. Ejdrup, A. M. D. Lee, H. Stapelfeldt, and A. Stolow, J. Chem. Phys. **125**, 234302 (2006).

- ¹³C. H. Jungen, D. N. Malm, and A. J. Merer, Can. J. Phys. **51**, 1471 (1973).
- ¹⁴Z. Li, M. Zhao, T. Xie, Y. Chang, Z. Luo, Z. Chen, X. Wang, K. Yuan, and X. Yang, Mol. Phys. **119**, 1813911 (2020).
- ¹⁵S. P. McGlynn, J. W. Rabalais, J. R. McDonald, and V. M. Scherr, Chem. Rev. 71, 73 (1971).
- ¹⁶S. C. Yang, A. Freedman, M. Kawasaki, and R. Bersohn, J. Chem. Phys. **72**, 4058 (1980).
- ¹⁷I. M. Waller and J. W. Hepburn, J. Chem. Phys. **87**, 3261 (1987).
- ¹⁸W.-B. Tzeng, H.-M. Yin, W. Y. Leung, J. Y. Luo, S. Nourbakhsh, G. D. Flesch, and C. Y. Ng, J. Chem. Phys. 88, 1658 (1988).
- ¹⁹T. N. Kitopoulos, C. R. Gebhardt, and T. P. Rakitzis, J. Chem. Phys. 115, 9727 (2001).
- ²⁰D. Xu, J. Huang, and W. M. Jackson, J. Chem. Phys. **120**, 3051 (2004).
- ²¹ G. Black, R. L. Sharpless, and T. G. Slanger, J. Chem. Phys. **66**, 2113 (1977).
- ²² Z. Li, M. Zhao, T. Xie, Z. Luo, Y. Chang, G. Cheng, J. Yang, Z. Chen, W. Zhang, G. Wu, X. Wang, K. Yuan, and X. Yang, J. Phys. Chem. Lett. 12, 844 (2021).
- ²³ J. L. Hardwick, Y. Ono, and J. T. Moseley, J. Phys. Chem. **91**, 4506 (1987).
- ²⁴M. Kawasaki, H. Sato, T. Kikuchi, A. Fukuroda, S. Kobayashi, and T. Arikawa, J. Chem. Phys. **86**, 4425 (1987).
- ²⁵ M. Kawasaki, H. Sato, S. Kobayashi, and T. Arikawa, Chem. Phys. Lett. **146**, 101 (1988).
- ²⁶S. P. Sapers and D. J. Donaldson, J. Phys. Chem. **94**, 8918 (1990).
- ²⁷S. P. Sapers and D. J. Donaldson, Chem. Phys. Lett. **198**, 341 (1992).
- ²⁸ Z. Zhang, Z. Chen, C. Huang, Y. Chen, D. Dai, D. H. Parker, and X. Yang, J. Phys. Chem. A 118, 2413 (2014).
- ²⁹ Z. Li, Y.-l. Fu, Z. Luo, S. Yang, Y. Wu, H. Wu, G. Wu, W. Zhang, B. Fu, K. Yuan, D. Zhang, and X. Yang, Science **383**, 746 (2024).
- ³⁰ Z. Zhang, H. Wu, Z. Chen, Y. Fu, B. Fu, D. H. Zhang, X. Yang, and K. Yuan, JACS Au. 3, 2855 (2023).
- ³¹Y. Chang, M. N. R. Ashfold, K. Yuan, and X. Yang, Natl. Sci. Rev. 10, nwad158 (2023).
- ³²S. Yang, Y. Wu, Z. Luo, Z. Li, W. Hua, Y. Chang, X. Wang, K. Yuan, and X. Yang, Chin. J. Chem. Phys. 37, 286 (2024).
- ³³B. Kleman, Can. J. Phys. **41**, 2034 (1963).
- ³⁴J. Zhou, Z. Luo, J. Yang, Y. Chang, Z. Zhang, Y. Yu, Q. Li, G. Cheng, Z. Chen, Z. He, L. Che, S. Yu, G. Wu, K. Yuan, and X. Yang, Phys. Chem. Chem. Phys. 22, 6260 (2020).
- 35 Z. Zhang, M. Xin, Y. Xin, S. Zhao, Y. Jin, G. Wu, D. Dai, Z. Chen, E. Sakkoula, D. H. Parker, K. Yuan, and X. Yang, Phys. Chem. Chem. Phys. 24, 25018 (2022).
- ³⁶ A. Stolow and Y. T. Lee, J. Chem. Phys. **98**, 2066 (1993).
- ³⁷K. Sato, Y. Achiba, H. Nakamura, and K. Kimura, J. Chem. Phys. 85, 1418 (1986).
- ³⁸ H. Kasahara, N. Mikami, M. Ito, S. Iwata, and I. Suzuki, Chem. Phys. **86**, 173 (1984).
- ³⁹G. E. Busch and K. R. Wilson, J. Chem. Phys. **56**, 3638 (1972).
- ⁴⁰ D. W. Neyer, A. J. R. Heck, D. W. Chandler, J. M. Teule, and M. H. M. Janssen, J. Phys. Chem. A **103**, 10388 (1999).
- ⁴¹T. V. Venkitachalam and A. S. Rao, Spectrochim. Acta, Part A 48, 1555 (1992).